Geoacoustic Inversion Using Back-propagation

Cheolsoo Park, Peter Gerstoft, Woojae Seong, *Member, IEEE,* and William S. Hodgkiss, *Member, IEEE*

***Abstract*—This paper presents inversion results of SW06 experimental data measured on a vertical line array (VLA1). The low frequency (100-900 Hz) chirp source was towed along two tracks (circle, straight line) at 30 m depth. For the inversions, a three-step optimization scheme is applied to the data using very fast simulated reannealing. The objective function is defined by the power of the back-propagated signal from the array to the source. At each step, water column sound speed profile, experimental geometry and geoacoustic parameters are inverted successively. An environmental model is employed consisting of a linear segmented sound speed profile in the water column, a sediment layer, and a half space. The geometric parameter inversion results show good agreement with *in situ* measurements. Finally, the estimated geoacoustic parameters show that the experimental site in the vicinity of VLA1 is fairly homogeneous in bottom properties consisting of a 21 m thick sediment layer with sound speed of around 1605 m/s over a hard basement whose sound speed is approximately 1750 m/s.**

***Index Terms*—Geoacoustic inversion, time domain inversion, back-propagation, SW06, multi-step optimization, VFSR.**

I. Introduction

GEOACOUSTIC inversion is a useful tool for estimating not only seabed properties but also other information such as source position, bathymetry and sound speed profile of the water column. The seabed properties are especially important in shallow water since sound propagation is strongly influenced by the bottom. Therefore, various methods for estimating the geoacoustic parameters of the ocean bottom via remote sensing have been developed.

This paper is focused on the broadband time domain inversion of nearfield (< 600 m) acoustic data. Most geoacoustic inversions have been performed in the frequency domain using either narrow or broad- band data [1,2]. However, the time domain approach has received attention as well [3-9].

When arrivals of different eigenrays are resolved, geoacoustic parameters can be inverted using travel times and/or amplitudes of measured and simulated data [6,9]. Otherwise, full waveform matching seeking the best correlation value between the measured and replica time series has been used [4,7]. The model based matched filter has also been a useful for time domain inversion [3,5].

It has been demonstrated that the sound wave received by a hydrophone, time reversed and retransmitted from the receiver position well focus at the source position [11]. This also has been explained as a matched filter [10], or generalized beamformer [12]. Numerically, equivalent processing can be implemented by back-propagating the time-reversed signal. The energy of the back-propagated signal, then becomes a measure of environmental mismatch, which can be used in source localization [12] and geoacoustic inversion [8].

A set of experiments (Shallow Water '06, SW06) was carried out in shallow water near the New Jersey shelf break in summer 2006 [13]. One objective of SW06 was the acoustic characterization of the ocean bottom using sources, covering various bands of frequency. This paper presents the inversion results from the low frequency chirp data (100-900 Hz) recorded by a vertical line array (VLA1) while the source was following circular and straight paths at ranges 200-600 m. The inversion approach is based on the method described in [8] that was applied to ship noise recorded on a horizontal towed array. The objective function used the inversion is defined using the power of the back-propagated signals from the array to the source. Then, a three-step optimization is applied to the objective function to find the optimum environmental parameters.

The paper is organized as follows. In Sec. II, we describe the experiments and the acoustic data. In Sec. III, the inversion scheme is presented including the derivation of the objective function. Sec. III presents inversion results for the two track events and Sec. IV summarizes the paper.

II. Description Of Experiments

A. The experiments

The experimental data was collected near the New Jersey continental shelf break [13]. The acoustic data were recorded on a Marine Physical Laboratory vertical line array (VLA1) located at (39°1.4771'N, 73°2.259'W) as shown in Fig. 1. VLA1 has 16 hydrophones with 3.75 m spacing. The bottom hydrophone (channel 1) was 8.2 m above the sea floor. The seabed constitutes of low speed clay over the so-called 'R'-reflector that is approximately 20 m below the sea floor [14-19].

During the experiment, the source was towed by the R/V Knorr at 0.5-1 knots on the two tracks shown in Fig. 1. The first track was a circle around the VLA1 with a nominal radius

Manuscript received April 0, 2009. This Work was supported by the Office of Naval Research under Grant No. N00014-05-1-0264.

C. Park and W. Seong are with Marne Physical Laboratory, Scripps Institution of Oceanography, La Jolla, CA, 92093 USA, on leave from the Maritime & Ocean Engineering Research Institute(MOERI)/Korean Ocean Research & Development Institute(KORDI), Daejeon 305-343 Korea and the Department of Ocean Engineering, Seoul National University, Seoul 151-742, Korea, respectively(e-mail: c4park@ucsd.edu, wseong@snu.ac.kr).

P. Gerstoft and W. S. Hodgkiss are with Marine Physical Laboratory, Scripps Institution of Oceanography, La Jolla, California 92093-0238 (e-mail: gerstoft@ucsd.edu, whodgkiss@ucsd.edu).

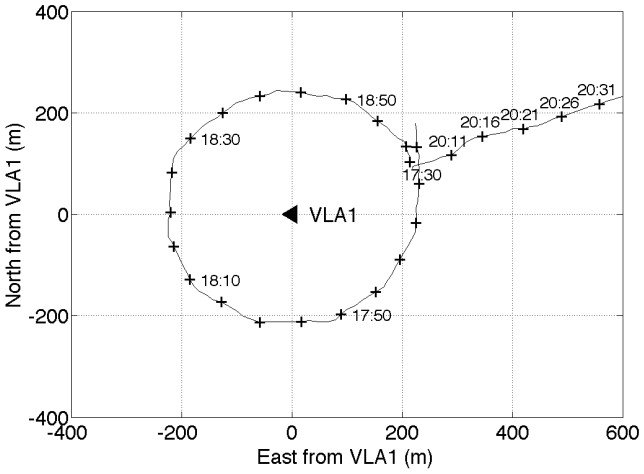

Fig. 1. The experimental configuration. Circular and straight paths with respect to VLA1 are shown. The tick interval is 5 minutes.

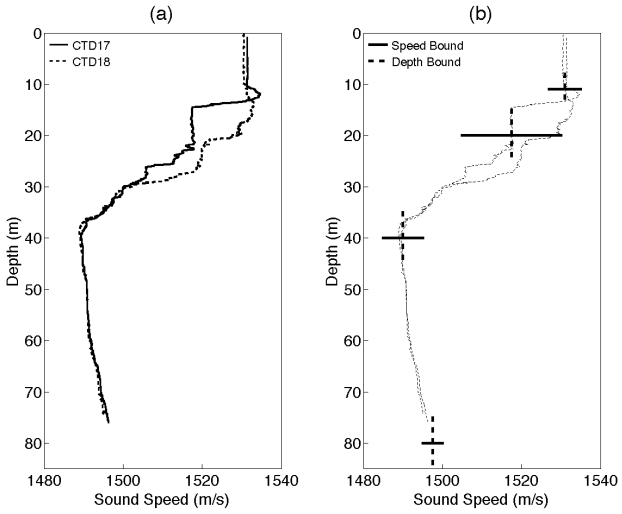

Fig. 2. The sound speed profiles (a) derived from CTD17 (19:17 UTC) and CTD18 (19:54 UTC). The water column SSP is modeled as a 4 segment linear sound speed profile for the inversion and the search bounds for the sound speeds and break points of each segment are shown in (b).

of 230 m. The second was a straight run. During both tracks, the source was at 30 m depth and emitting continuously a 1 s LFM transmission swept from 100 to 900 Hz. The bathymetry along the tracks was almost flat with a water depth of roughly 79 m.

The circle event started at 17:25 UTC (Coordinated Universal Time) 27 August 2006 and finished at 19:00 UTC. The straight event was carried out from 20:07 to 21:30 UTC. Two CTDs (Conductivity-Temperature-Depth), CTD17 and CTD18, were obtained near VLA1 during this period. Fig. 2 (a) shows the water column sound speed profiles (SSPs) derived from the two CTDs. Significant differences between two SSPs are observed between depths of 10 m and 30 m where fluctuations in the thermocline region are found.

B. Acoustic data processing

The raw data obtained from 16 VLA1 were matched filtered using a synthetic 1-s 100-900 Hz LFM waveform. The sampling rate was reduced to 10 kHz (down-sampled from 50 kHz). The resulting compressed matched filtered data are used for the inversions. A single 1-s transmission was used for each inversion.

III. Inversion Approach

A. Objective function using back-propagation

In an ideal linear time invariant system without noise, the propagation of a source signal $s(t)$, e.g., a chirp signal [7] or ship noise [8], from a source $\mathbf{r}_s$ to a receiver $\mathbf{r}_r$ through a medium expressed by the vector $\mathbf{m}_0$, is given by the convolution with the medium impulse response $h(t)$ as

$$d(t,\mathbf{r}_s,\mathbf{r}_r,\mathbf{m}_0) = s(t) * h(t,\mathbf{r}_s,\mathbf{r}_r,\mathbf{m}_0), \quad (1)$$

where $d(t,\mathbf{r}_s,\mathbf{r}_r,\mathbf{m}_0)$ is the received signal by a hydrophone and * is the convolution operator. If the received signal is time reversed and propagated from the receiver to the source position, the back-propagated signal becomes

$$\begin{aligned} b(t,\mathbf{r}_r,\mathbf{r}_s,\mathbf{m}_0) &= d(T-t,\mathbf{r}_s,\mathbf{r}_r,\mathbf{m}_0) * h(t,\mathbf{r}_r,\mathbf{r}_s,\mathbf{m}_0) \\ &= s(T-t) * \left(h(T-t,\mathbf{r}_s,\mathbf{r}_r,\mathbf{m}_0) * h(t,\mathbf{r}_r,\mathbf{r}_s,\mathbf{m}_0)\right), \end{aligned} \quad (2)$$

where T is a maximum time extent of the received signal. Since due to reciprocity the source and receiver position can be exchanged, the $h(T-t,\mathbf{r}_s,\mathbf{r}_r,\mathbf{m}_0) * h(t,\mathbf{r}_r,\mathbf{r}_s,\mathbf{m}_0)$ in (2) is a time delayed auto-correlation of the impulse response $h(t,\mathbf{r}_s,\mathbf{r}_r,\mathbf{m}_0)$. Therefore, the back-propagated signal is equivalent to the convolution between the source and the auto-correlation of the impulse response.

Figs. 3 and 4 show simulations of the back-propagation for an 80-m deep Pekeris waveguide. The sound speeds of the water column and the bottom are 1500 and 1600 m/s, respectively. The bottom density is 1.8 g/cm^3. The 100-900 Hz source is located at 30 m depth and 230 m range from the VLA1. Fig. 3(b), (c) and (d) are the auto-correlation of the impulse responses for channel 1, 8 and 16, respectively. Fig. 3(a) is the sum of auto-correlations for all 16 channels. Amplitudes are normalized such that the maximum is 1. It can be seen from Fig. 3(b), (c) and (d) that the auto-correlation for an individual channel contains a main lobe and multiple side lobes. If the auto-correlations for different channels are added coherently in time, the main lobe will be reinforced whereas the side lobes are cancelled by destructive interference. As a result, the main lobe becomes dominant and approaches the band-limited impulse response of free space when the number of channels is large as shown in Fig. 3 (a).

Although we used matched filtered LFM signals for the inversion, (1) and (2) are general. For a clear understanding of the characteristics of time-reversed back-propagation, therefore, a first derivative Gaussian waveform is used as an example instead of the symmetrical matched filtered LFM source. The first derivative Gaussian waveform, $(t-t_0)\exp(-(t-t_0)^2)$, is shown in Fig. 4 (a). The source

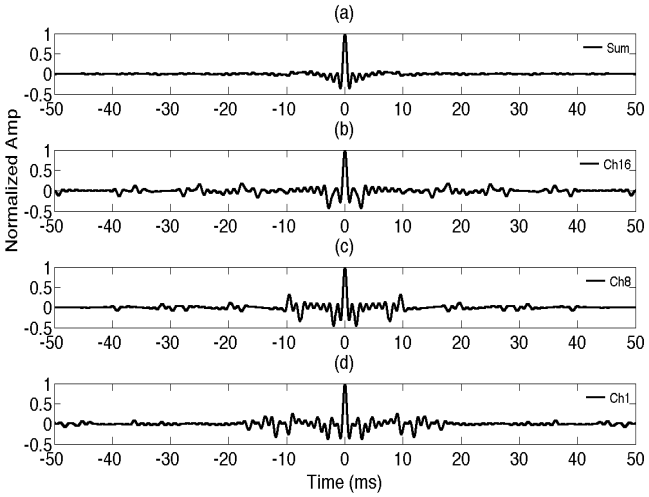

Fig. 3. Auto-correlation of the impulse responses: (a) sum of all 16 hydrophones, (b) channel 16, (c) channel 8, (d) channel 1.

signal is band-pass filtered over 100-900 Hz. The waveform of the sum of back-propagated signals for all channels is shown (solid) in Fig. 4 (b). The auto-correlation of the impulse response is also shown (dashed) as a reference. Amplitudes for all plots are normalized to 1. It is evident that the resulting back-propagated waveform becomes similar to the time-reversed source waveform since the sum of impulse response auto-correlations approach that of the band-limited impulse response of free space.

For geoacoustic inversion, a replica can be substituted for the true impulse response. When the environment for the replica is the same as the true environment, the back-propagated signal will focus spatially at the original source position with the waveform being approximately equal to the time-reversed source signal.

Inversion parameters describing the environment (including source/receiver parameters) are represented by the replica model vector $\mathbf{m} = \left[m_1, m_2, ..., m_{N_m}\right]^T$, where $[]^T$ is the transpose operator and N_m is the number of parameters. The normalized back-propagated signal is defined as [8]

$$b_n(t,\mathbf{m}) = \frac{1}{N_r}\sum_{k=1}^{Nr} \frac{d_k(T-t)}{\sqrt{\int_0^T |d_k(\tau)|^2 d\tau}} * \frac{h_k(t,\mathbf{m})}{\sqrt{\int_0^T |h_k(\tau,\mathbf{m})|^2 d\tau}} \qquad (3)$$

where $d_k(t)$ and $h_k(t,\mathbf{m})$ are the measured signal and replica for the kth hydrophone of the N_r element array, and T is the maximum time extent of the signals. The purpose of the normalization in (3) is to remove the dependency on the energy of the source and replica in the cross-correlation.

If the data $d_k(t)$ is the impulse response measured [3] or estimated [5], maximizing (3) over the whole time lag t becomes similar to the objective function employed in time series matching inversions [3,4,5,7]. Here, the objective function to be maximized for the inversion is defined as

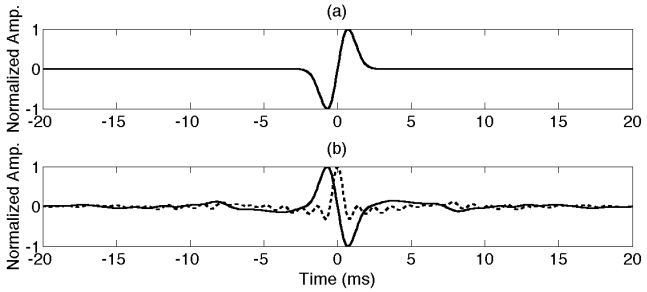

Fig. 4. (a) Source waveform and (b) back-propagated signal at the source position (solid) along with the sum of the auto-correlations of impulse responses (dashed).

$$\phi(\mathbf{m}) = \max_{t_1}\left[\int_{t_1}^{t_1+\Delta t} |b_n(t,\mathbf{m})|^2 dt\right], \text{ for } 0 \le t_1 \le T - \Delta t. \qquad (4)$$

The Δt is a focal time-width of the back-propagated signal and depends on the source waveform such that most energy of the source is confined within Δt [8,12]. The spatial resolution of time-reversal is described in [13].

An influential factor in the correlation of signals is time delay. Mismatches in time delays result in a considerable reduction of correlation, but the signal amplitudes have little effect. Therefore, the inversion parameters that influence the time delay of the signals such as source-receiver positions, water depth, layer thickness, and sound speed usually show higher sensitivities than those mostly influencing the amplitude such as densities and attenuations.

B. Inversion scheme

The raw acoustic data at a hydrophone of VLA1, ignoring noise, is

$$r(t) = s_0(t) * h(t), \qquad (5)$$

where $s_0(t)$ is 1-s LFM (100-900 Hz) signal. The matched filtered signal becomes

$$d(t) = s_0(-t) * r(t) = \left(s_0(-t) * s_0(t)\right) * h(t) = s(t) * h(t), \qquad (6)$$

where $s(t)$ is now the compressed wavelet of the LFM signal, which is equivalent to (1). In the following, the acoustic data refers to the matched filtered signal in (6).

Inversion parameters are categorized into three groups: geometric, geoacoustic, and sound speed profile (SSP) groups. The geometric group includes the source depth, source range, tilt of VLA1, and water depth. The geoacoustic group consists of the parameters describing the bottom such as sound speed, density, and layer thickness. Based on the model for the experimental site near the VLA1 [9,18,20], a range independent model with a sediment layer over a half space is adopted. Therefore, the geoacoustic parameters are sound speeds and densities of the sediment layer and the half space and a layer thickness. Sound speeds of the bottom are assumed constant in each layer. Attenuation is excluded due to its low sensitivity at mere short ranges.

The water column SSP shows significant variability both in time and space. Also, the CTD measurements were not preformed simultaneous with the acoustic measurements. The measured SSP in Fig. 2 (a) is composed of 3 sub-regions: upper constant region, thermocline region with multiple gradients, and lower iso-gradient region. Here, the water column is divided into 4 segments: one for upper iso-speed region, two for thermocline, and one for lower iso-gradient region. The sound speed is modeled as a linear profile in each segment and discontinuity is not allowed at the segment break points. The search bounds for the break points are shown in Fig. 2 (b).

The inversion is performed via an optimization process that searches the parameters to maximize the objective function $\phi(\mathbf{m})$ in (4). Direct and surface reflected signals usually have large amplitudes. But they contain mostly the geometric and the ocean SSP information and thus do not contribute directly to the inversion of bottom properties. If all the parameters are inverted simultaneously, the geometric parameters or the SSP parameters dominate over the geoacoustic parameters in the search process. In order to prevent this, it is desired that the parameters be inverted separately based on their sensitivities. The multi-step inversion also reduces the number of parameters in each step incorporating an efficient optimization [21].

A 3-step approach is applied to the inversion as follows:

(1) The target parameters are the SSP group. At first, the inversion is carried out using a simple half space model whose parameters are the SSP group, the geometric group, and the sound speed of the bottom. Since bottom density is not important, it is fixed at 2.0 g/cm^3. Although the final bottom model is sediment layer over a half space, the simple half space model used in the first step is chosen for efficiency. Among all the inverted parameters, only the SSP parameters are passed to the next inversions.

(2) The target parameters are the geometric group. The inversion still is carried out using the simple half space model. The inversion parameters are the geometric and geoacoustic parameters. The inverted geometric parameters along with the SSP parameters are passed to the final inversion.

(3) The final inversion is carried out for the geoacoustic parameters using the sediment layer over a half space bottom model.

In all inversions, the very fast simulated reannealing (VFSR [22]) global search algorithm is used. This is a modified version of simulated annealing (SA) and has been useful in geophysical and geoacoustic applications [7,23]. It consists of successive quenching sequences where the quenching temperature is lowered according to a pre-determined schedule. We applied 50 successive quenching sequences to the first and the second steps and 100 quenching sequences to the third step of the inversion. For each sequence, 50 parameter evaluations are carried out. Therefore, 10000 replica calculations are performed for the entire inversion.

For the forward model, a ray-based time domain modeling method is used, see the Appendix.

IV. INVERSION RESULTS

The signal truncation time, T in (3), is chosen as 1 s so that all the arrivals are included within it. Most of the power of the matched filtered 100-900 Hz chirp was concentrated in the main lobe of 2 ms width. Therefore, the focal time-width, Δt in (4), is set to 2 ms. Note, that a single ping was used for each

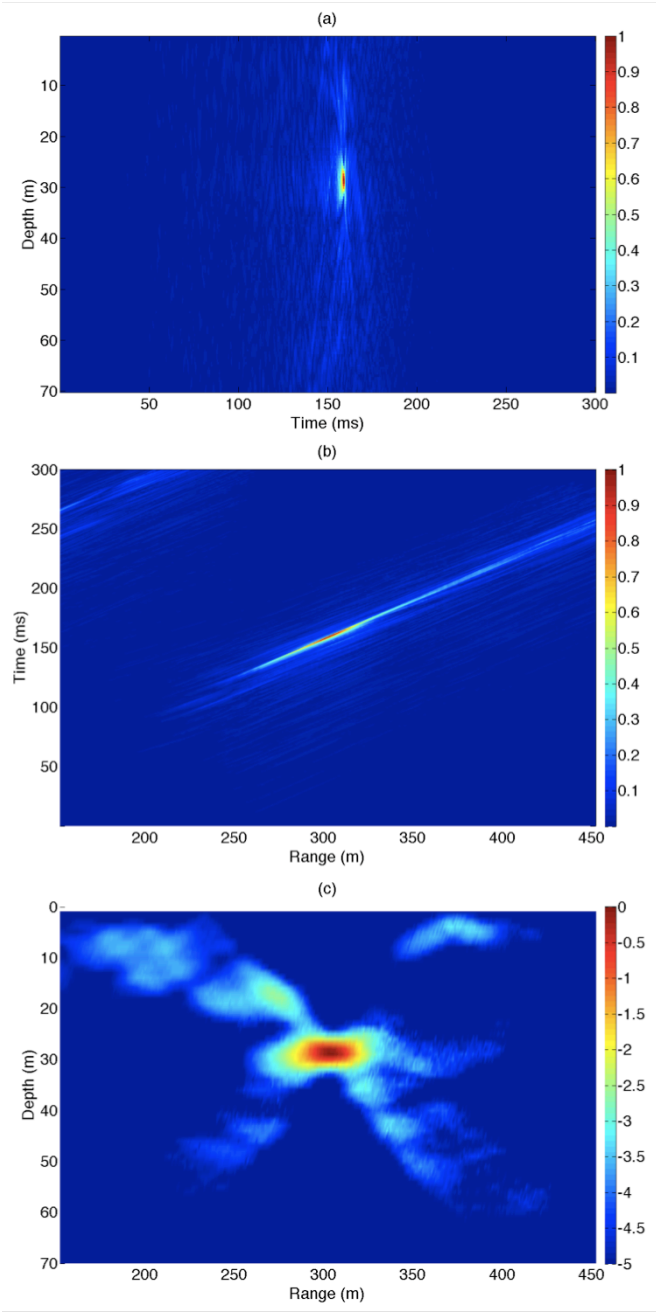

Fig. 5. Envelopes of back propagated array data in (3) with varying (a) depth and (b) range. (c) ambiguity surface of the objective function in (4) (dB) using Δt = 2 ms.

inversion. It is expected that the acoustic data will show temporal variations due to environmental effects such as SSP fluctuation and surface wave activity.

A. Back-propagation and parameter sensitivity

To understand the characteristics of back-propagation of the received signals, we simulated the back-propagated signals from the VLA1 to candidate source positions using inverted environment for the data at 20:12 UTC. Fig. 5(a) and (b) show the envelopes of the back-propagated array data [$b_n(t,\mathbf{m})$ in (3)] as a function of depth and range, while the other parameters are those obtained in the inversion. The inverted source range is 302 m and depth is 28.5 m. The amplitudes are normalized to a maximum of 1. Since the acoustic data are compressed as in (6), the back-propagated signal is also compressed. From the figure, a strong main lobe with minor side lobes is observed around the inverted source position. The focusing of the signal is mainly due to the constructive interference and spatial coherence of the auto-correlations. The ambiguity surface in Fig. 5 (c) [$\phi(\mathbf{m})$ in (4)], shows a good focus of the back-propagated array data at the correct source position. The matched filtered array data at 20:12 UTC and the simulated impulse response using the inverted parameters are shown in Fig. 6.

A set of geometric and geoacoustic parameter inversion

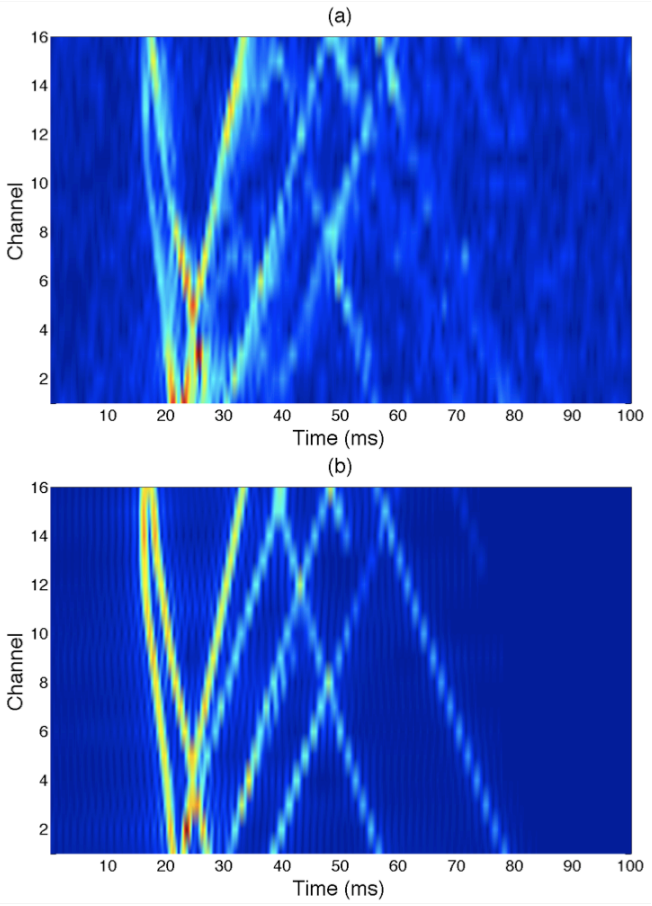

Fig. 6. Envelopes of (a) matched filtered array data at 20:12 UTC and (b) impulse response simulated using inversion results.

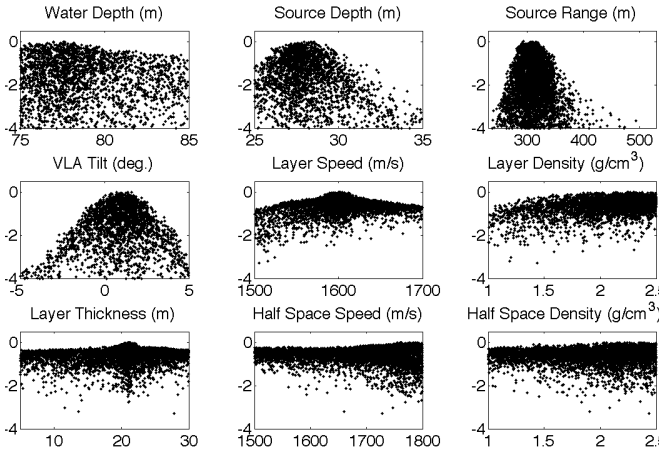

Fig. 7. Scatter plots of the VFSR search for array data at 20:12 UTC. The y-axis of the plot is relative power (dB) of the objective function value evaluated during the optimization and the x-axis spans the parameter search bound.

results for the data at 20:12 UTC is presented as scatter plots in Fig. 7. The scatter plots represent the relative power (dB) of the objective function (y-axis) for the corresponding parameter (x-axis) evaluated during optimization. The scatter plots give information on the behavior of parameters such as sensitivity and coupling [8]. If the objective function is sensitive to a parameter, it decreases rapidly from the maximum.

The geometric parameters commonly show high sensitivities. Among the geoacoustic parameters, the sediment layer parameter is more sensitive than the half space parameters. There are distinct maxima both in layer sound speed and in thickness of the layer of around 1600 m/s and 21 m, respectively.

B. Circle Event

This section presents the results of the inversions for the circle event. The circle event was carried out for 1.5 hours from 17:25 to 19:00 UTC, see Fig. 1. Twenty 1-s long records of acoustic data at 5-minute intervals are inverted.

Fig. 8 shows the inverted parameters. The search bounds span the y-axis range for each parameter except for the SSP described in Section III. B (see Fig. 2(b)). During the event, some geometrical parameters such as source range, source depth and water depth were measured *in situ* with nominal values 230, 30 and 79 m, respectively. These values agree well with the inversion results. The source range estimated from the ship DGPS is compared with the inverted range on the plot. The inverted tilt angle shows a periodic pattern, as expected for the circle. According to the tilt meter on the VLA1, the tilt angle was 1.8 ± 1° during the circle event. The absolute value of the peak inverted tilt angles are within the range of the measured tilts.

The inversion results for the geoacoustic parameters supports the conclusion that the seabed around the site consists of a low speed layer over a high-speed reflector. The experimental site even appears to be homogeneous in terms of the bottom properties with the inverted sound speeds of the

bottom and layer thicknesses showing little variability for the sampled data. The statistics (mean ± standard deviation) for the geoacoustic parameter estimates from 20 samples of acoustic data are given in Table I. The seabed around VLA1 is homogeneous and is composed of a 21.2 m thick layer sediment with sound speed 1606 m/s over the so-called 'R'-reflector with wound speed 1740 m/s.

The inverted sound speeds of the water column show large fluctuations especially in the thermocline. For the SSP inversion, an alternative would be to use an empirical orthogonal function (EOF) model [9,20,24].

The normalized powers (dB) of the maximum objective function values obtained at all 3 steps of each inversion are given in the lower-middle panel of Fig. 8. The powers become higher as the inversion step advances, which is expected with the multi-step inversion.

C. *Straight Event*

This section presents the results of the inversions during the straight event from 20:11 to 20:30 UTC, see Fig. 1. Twenty 1-s long records of acoustic data at 1 minute intervals from 21:11 UTC are inverted.

Fig. 9 shows the inverted parameters for the straight event. The search bounds are the same as for the circle event except for the source range. The search bounds of the range are 380 ±

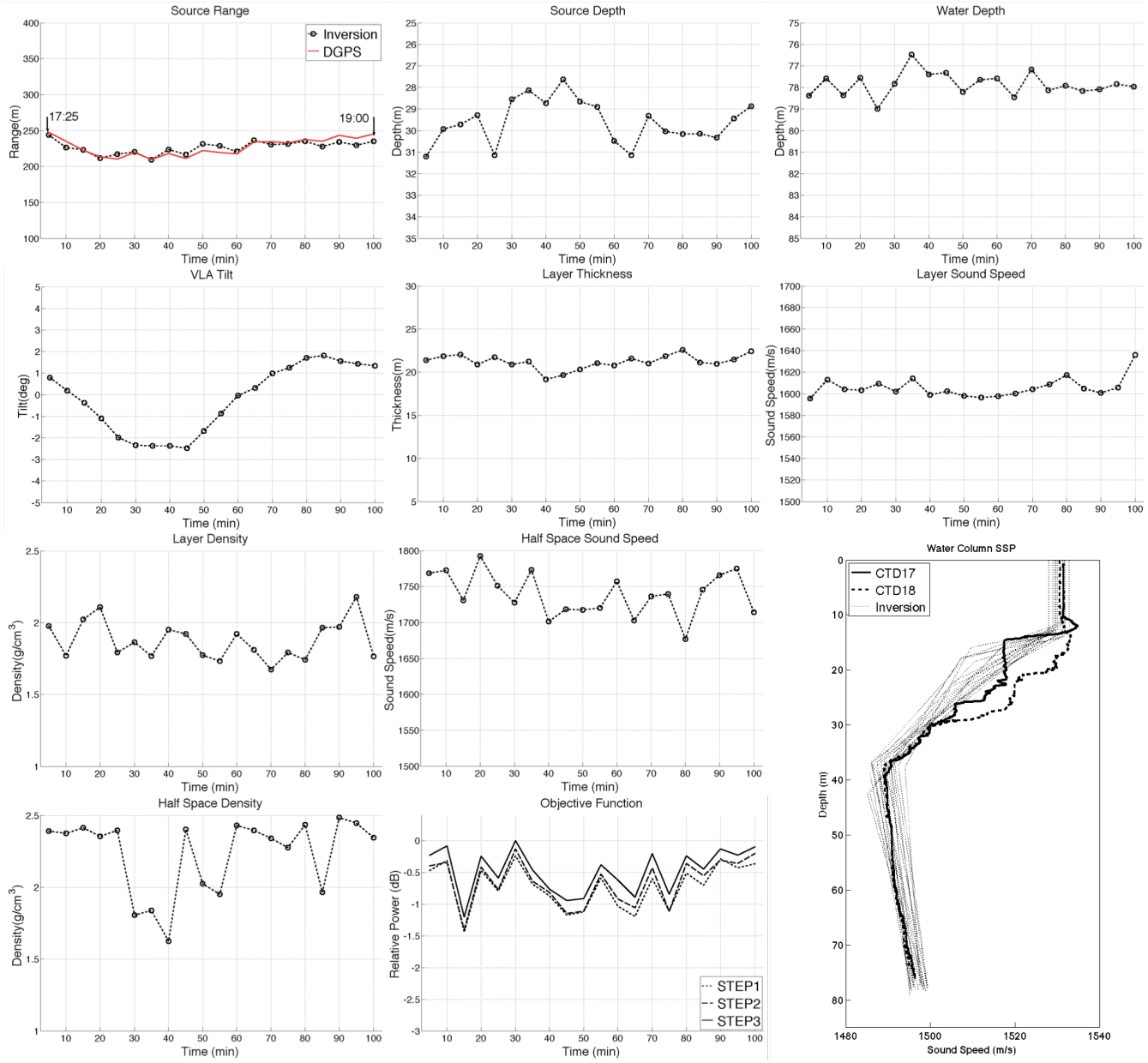

Fig. 8. Inversion results from the circle event (17:25 to 19:00 UTC). In the plot of source range, the range estimated from the ship DGPS is compared with the inverted range.

150 m for the first half of the data and 530 ± 150 m for the rest. The nominal source depth is 30 m and water depth is 79 m. The inverted and nominal values for the geometrical parameters match well. As a reference, the range of the source obtained from the onboard DGPS is also given in the inverted source range plot. Comparing two data validates the inversion results. The tilt angle measured from 20:11 to 20:30 UTC was 1.6 ± 1°. The projected tilt onto the vertical plane of the ship trajectory corresponds to 1.5° and agrees with the inverted angle.

The inversion results for the geoacoustic parameters of the straight event also support the conclusion that the seabed around the array site consists of a low speed sediment layer over a high-speed reflector. The statistics (mean ± standard deviation) for the geoacoustic parameter estimates from 20 samples of acoustic data also are given in Table I. The seabed structure along the straight track is homogeneous and is composed of the 21.3 m thick sediment layer with sound speed 1601 m/s over the so-called 'R'-reflector with sound speed 1761 m/s.

V. Conclusion

Time domain geoacoustic inversion results for SW06 experimental data (100-900 Hz chirps) are presented for near field measurements with a source range less than 600 m. For the inversion, the objective function was defined as the power

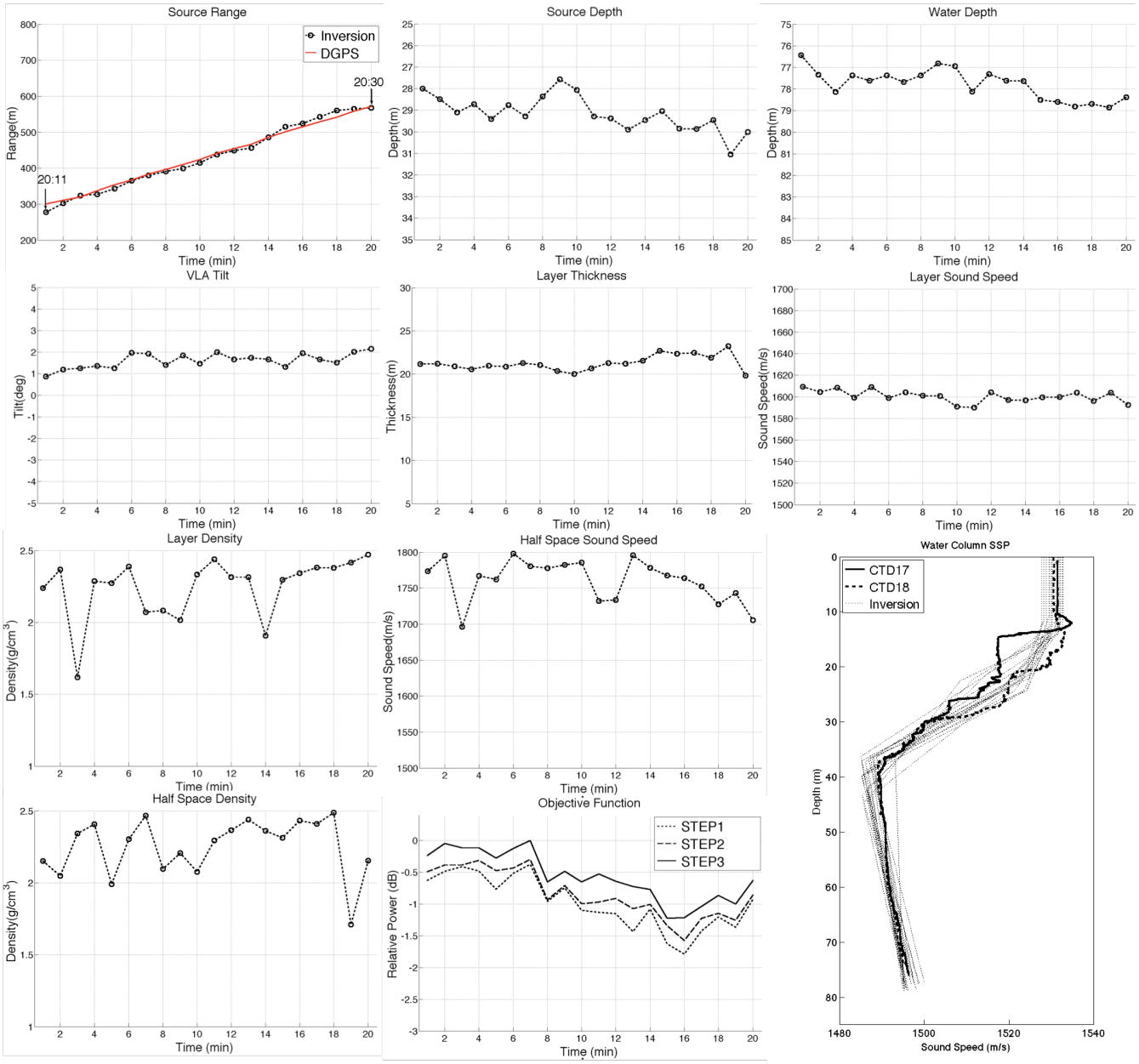

Fig. 9. Inversion results from the straight event (20:11 to 20:30 UTC). In the plot of source range, the range estimated from the ship DGPS is compared with the inverted range.

of back-propagated acoustic array data from VLA1 to the source. A three-step inversion scheme was applied to the data and the VFSR algorithm was used as an optimizer for the objective function.

The inversion results from the circle event showed that the geoacoustic properties around VLA1 are homogeneous and the bottom is composed of a 21.2 m thick sediment layer with low sound speed (1606 m/s) over the faster 'R'-reflector (1740 m/s). The inversion results form the straight run also yielded similar results estimating a 21.3 m sediment layer (1601 m/s sound speed) and faster subbottom (1761 m/s sound speed).

APPENDIX

A. The forward model

A ray-based forward model is used to simulate waveforms in the time domain and it is implemented as follows. The acoustic data received at a hydrophone consist of coherent signals from distinct eigenray paths. The impulse response is a function of the amplitudes and the phases of their paths. The phase is determined both by the travel times of the eigenrays and by complex reflection coefficients.

At first, a ray is assumed to be emanating from the source with incident angle θ_i through a medium with a linear sound speed profile such as

$$c(z) = c(z_1) + a(z - z_1), \quad z_1 \le z \le z_2, \tag{A1}$$

where $c(z_1)$ is the sound speed at a depth of z_1 and a is the constant gradient of the SSP. According to Snell's law, the travel length and the travel time between a start point z_i and an end point z_f become

$$L_{i\_f} = \frac{c(z_i)}{a\sin(\theta_i)}\Big(\cos(\theta_i) - \cos(\theta_f)\Big), \tag{A2}$$

$$t_{i\_f} = \frac{1}{a}\log_e \frac{\Big(z_f - z_1 + c(z_1)/a\Big)\Big(1 + \cos(\theta_i)\Big)}{\Big(z_i - z_1 + c(z_1)/a\Big)\Big(1 + \cos(\theta_f)\Big)}. \tag{A3}$$

When the ray reaches an interface, call it a branch point, it reflects and transmits with changes in both the propagation angles and amplitudes. If we ignore geometrical spreading for the time being and assume a planar interface, the angles and the amplitudes are easily calculated. The branch points are tracked and stored until the ray reaches the receiver range. The ray is determined as an eigenray if it arrives at the receiver position within a predetermined error bound. Considering geometrical spreading loss, the complex amplitude of the eigenray having N_b branch points is calculated by

$$A_{eigen}(f) = \frac{1}{L_{tot}}\prod_{i=1}^{N_b} A^i_{branch}\exp\left(-\frac{\alpha_i}{40\pi\log e}k_i(f)L^i_{branch}\right), \tag{A4}$$

where L_{tot} and L^i_{branch} are travel lengths from the source to the receiver and between adjacent branch points, respectively. A^i_{branch} is the reflection or transmission coefficient depending on the propagation pattern of the eigenray. In addition, $\alpha_i(dB/\lambda)$ is the attenuation coefficient and $k_i(f)$ is the wavenumber for a frequency f. Finally, the discrete impulse response for all N_e eigenrays becomes

$$h(t) = \mathrm{Re}\Big(\int_{f_1}^{f_2}\sum_{i=1}^{N_e} A^i_{eigen}(f)\exp(i2\pi f(t - \tau^i_{tot}))df\Big)\Big/(f_2 - f_1), \tag{A5}$$

where τ_{tot} is a travel time between the source and the receiver and f_1 and f_2 are the minimum and maximum frequencies of the broadband source, respectively. Removing the frequency dependence of (A4) by approximating the wavenumber as that at the center frequency, (A5) can be calculated as

$$h(t) = \sum_{i=1}^{N_f}\frac{\left|A^i_{eigen}\right|}{f_{\max} - f_{\min}}\left[\frac{\sin(2\pi f_2(\tau^i_{tot} - t) + \phi_i)}{\pi(\tau^i_{tot} - t)} - \frac{\sin(2\pi f_1(\tau^i_{tot} - t) + \phi_i)}{\pi(\tau^i_{tot} - t)}\right], \tag{A6}$$

where $\left|A^i_{eigen}\right|$ and ϕ_i represent the amplitude and phase of A^i_{eigen}.

REFERENCES

[1] C. F. Mecklenbräuker and P. Gerstoft, "Objective functions for ocean acoustic inversion derived by likelihood methods," *J. Comp. Acoust.,* vol. 48(2), pp. 259-270, 2000.

[2] J-P. Hermand and P. Gerstoft, "Inversion of broadband multitonal acoustic data from the yellow shark summer experiments," *IEEE J. Oceanic Eng*., vol. 21, pp. 324-346, 1996.

[3] J-P. Hermand, "Broad-band geoacoustic inversion in shallow water from waveguide impulse response measurements on a single hydrophone: theory and experimental results," *IEEE J. Oceanic Eng*., vol. 24, pp. 41-66, 1999.

[4] L. Jaschke and N. R. Chapman, "Matched field inversion of broadband data using the freeze bath method", *J. Acoust. Soc. Amer*., vol. 106(4), pp. 1838-1851, 1999.

[5] Z-H. Michalopoulou, "Matched-impulse-response processing for shallow-water localization and geoacoustic inversion," *J. Acoust. Soc. Amer*., vol. 108(5), pp. 2082-2090, 2000.

[6] P. Pignot and N. R. Chapman, "Tomographic inversion of geoacoustic properties in a range-dependent shallow-water environment," *J. Acoust. Soc. Amer*., vol. 110(3), pp. 1338-1348, 2001.

[7] C. Park, W. Seong, P. Gerstoft, and M. Siderius, "Time domain geoacoustic inversion of high-frequency chirp signal from a simple towed system," *IEEE J. Oceanic Eng*., vol. 28, pp. 468-478, 2003.

[8] C. Park, W. Seong, and P. Gerstoft, "Geoacoustic inversion in time domain using ship of opportunity noise recorded on a horizontal towed array," *J. Acoust. Soc. Amer.*, vol. 117(4), pp. 1933-1941, 2005.

[9] Y-M. Jiang, N. R. Chapman, and P. Gerstoft, "Short range geoacoustic inversion with vertical line array," *J. Acoust. Soc. Amer*., vol. 124(3), Pt. 2 of 2, EL135 - EL140, 2008.

[10] C. S. Clay, "Optimum time domain signal transmission and source localization in a wave guide," *J. Acoust. Soc. Amer.*, vol. 81(3), pp. 660-664, 1987.

[11] A. Parvulescu and C. S. Clay, "Reproducibility of signal transmission in the ocean," *Radio Electron. Eng.*, vol. 29, pp. 223-228, 1965.

[12] R. K. Brienzo and W. S. Hodgkiss, "Broadband matched-field processing," *J. Acoust. Soc. Amer.*, vol. 94(5), pp.2821-2831, 1993.

[13] S. Kim, G. F. Edelmann, W. A. Kuperman, W. S. Hodgkiss, and H. C. Song, "Spatial resolution of time-reversal arrays in shallow water," *J. Acoust. Soc. Amer*., vol. 110(2), pp. 820-829, 2001.

[14] D. J. Tang, J. Moum, J. Lynch, P. Abbot, R. Chapman, P. Dahl, T. Duda, G. Gawarkiewicz, S. Glenn, J. Goff, H. Graber, J. Kemp, A. Maffei, J. Nash, and A. Newhall, "Shallow Water '06 - a joint acoustic

propagation / nonlinear internal wave physics experiment," *Oceanogr.*, vol. 20(4), pp. 156–167, 2007.
[15] T. A. Davies, J. A. Austin, Jr., M. B. Lagoe, and D. Milliman, "Late quaternary sedimentation off New Jersey: new results using 3-D seismic profiles and cores," *Marine Geology*, Vol. 108, pp. 323-343, 1992.
[16] A. Turgut, D. Lavoie, D. J. Walter, and W. B. Sawyer, "Measurements of bottom variability during SWAT New Jersey Shelf Experiments," in *Impact of Littoral Environmental Variability on Acoustic Predictions and Sonar Performance*, Kluwer academic publishers, 2002, pp. 91-98.
[17] J. A. Goff, B. J. Kraft, L. A. Mayer, S. G. Schock, C. K. Sommerfield, H. C. Olson, S. P.S. Gulick, and S. Nordfjord, "Seabed characterization on the New Jersey middle and outer shelf: correlatability and spatial variability of seafloor sediment properties," *Marine Geology*, vol. 209, pp. 147-172, 2004.
[18] Y-M. Jiang, N. R. Chapman, and M. Badiey, "Quantifying the uncertainty of geoacoustic parameter estimates for the New Jersey shelf by inverting air gun data," *J. Acoust. Soc. Amer.*, vol. 121(4), pp. 1879-1894, 2007.
[19] J. W. Choi, P. H. Dahl, and J. A. Goff, "Observations of the R reflector and sediment interface reflection at the Shallow Water '06 Central Site," *J. Acoust. Soc. Amer*., vol. 124, EL128 - EL134, 2008.
[20] C. F. Huang, P. Gerstoft, and W. S. Hodgkiss, "Effect of ocean sound speed uncertainty on matched-field geoacoustic inversion," *J. Acoust. Soc. Amer.*, vol. 123, EL162 - EL168, 2008.
[21] P. Ratilal, P. Gerstoft, and J. T. Goh, "Subspace approach to inversion by genetic algorithms involving multiple frequencies," *J. Comp. Acoust.,* vol. 6, pp. 99-115, 1998.
[22] L. Ingber, "Very fast simulated reannealing," *Math. Comput. Modeling*, vol. 12(8), pp. 967-993, 1989.
[23] M. K. Sen and P. L. Stoffa, *Global optimization methods in geophysical inversion*, Elsevier, Amsterdam, The Netherlands, 1995.
[24] P. Gerstoft and D. F. Gingras, "Parameter estimation using multifrequency range-dependent acoustic data in shallow water," *J. Acoust. Soc. Amer.*, vol. 99(5), pp. 2839-2850, 2007.

TABLE I
INVERTED GEOACOUSTIC PARAMETERS FOR THE CIRCLE AND STRAIGHT EVENTS

CASE	Layer			Half Space	
	Speed (m/s)	Density (g/cm^3)	Thickness (m)	Speed (m/s)	Density (g/cm^3)
Circle	1606 ± 9	1.9 ± 0.1	21.2 ±0.8	1740 ±30	2.2 ±0.3
Straight	1601 ± 6	2.3 ± 0.2	21.3 ±0.9	1761 ±29	2.3 ±0.2